Title

Artificial Intelligence Approach for Estimating Dairy Methane Emissions

Journal

Environmental Science and Technology, 56(8)

ISSN

0013-936X

Authors

Jeong, Seongeun
Fischer, Marc L
Breunig, Hanna
et al.

Publication Date

2022-04-19

DOI

10.1021/acs.est.1c08802

Peer reviewed

Environmental Science & Technology

pubs.acs.org/est

Article

Artificial Intelligence Approach for Estimating Dairy Methane Emissions

Seongeun Jeong,* Marc L. Fischer, Hanna Breunig, Alison R. Marklein, Francesca M. Hopkins, and Sebastien C. Biraud

Cite This: *Environ. Sci. Technol.* 2022, 56, 4849−4858

Read Online

ACCESS | Metrics & More | Article Recommendations | Supporting Information

ABSTRACT: California's dairy sector accounts for ∼50% of anthropogenic CH_4 emissions in the state's greenhouse gas (GHG) emission inventory. Although California dairy facilities' location and herd size vary over time, atmospheric inverse modeling studies rely on decade-old facility-scale geospatial information. For the first time, we apply artificial intelligence (AI) to aerial imagery to estimate dairy CH_4 emissions from California's San Joaquin Valley (SJV), a region with ∼90% of the state's dairy population. Using an AI method, we process 316,882 images to estimate the facility-scale herd size across the SJV. The AI approach predicts herd size that strongly (>95%) correlates with that made by human visual inspection, providing a low-cost alternative to the labor-intensive inventory development process. We estimate SJV's dairy enteric and manure CH_4 emissions for 2018 to be 496−763 Gg/yr (mean = 624; 95% confidence) using the predicted herd size. We also apply our AI approach to estimate CH_4 emission reduction from anaerobic digester deployment. We identify 162 large (90th percentile) farms and estimate a CH_4 reduction potential of 83 Gg CH_4/yr for these large facilities from anaerobic digester adoption. The results indicate that our AI approach can be applied to characterize the manure system (*e.g.*, use of an anaerobic lagoon) and estimate GHG emissions for other sectors.

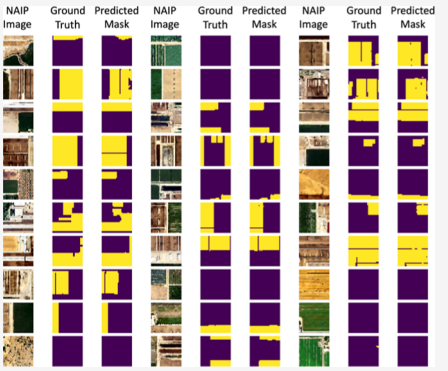

KEYWORDS: *artificial intelligence, methane, greenhouse gas, emission, dairy, aerial image*

1. INTRODUCTION

Methane (CH_4) is a short-lived greenhouse gas (GHG) and is about 80 times more potent over a 20 year time scale than carbon dioxide (CO_2).[1] In California, accounting for CH_4 emissions is essential because California committed to reducing GHG emissions through a series of legislations, including Senate Bill 32 requiring statewide emissions to be 40% below 1990 levels by 2030.[2] Specific to source emissions, Senate Bill 1383 requires reducing CH_4 emissions from dairy manure management by 40% below the 2013 levels by 2030.[3] Because California's dairy accounts for ∼50% of the state's total anthropogenic CH_4 emissions,[4] quantifying dairy CH_4 emissions is critical for implementing California's climate change laws. Due to California's position (∼20% of the US total[5]) in the US dairy industry, understanding California's dairy CH_4 can offer useful emission quantification and mitigation strategies beyond the state level.

Many CH_4 emission quantification studies have been conducted in California using multiplatform atmospheric measurements, including ground and satellite observations. As a result, the state total CH_4 emission estimates started converging, with different studies reporting statistically consistent estimation results.[6,7] However, quantifying dairy-specific CH_4 emissions, separate from other sources, remains a challenge due to substantial uncertainties associated with emission estimation.[7] One remedy to this considerable uncertainty in dairy CH_4 quantification is to use a spatially accurate representation of dairy facilities in time and space. In this work, a dairy facility represents the whole farm, typically associated with enteric (*e.g.*, a free stall barn) and manure (*e.g.*, an anaerobic lagoon) emission sources.

Although dairy facilities' size varies over time, recent inverse modeling studies in California continue to use decade-old facility-scale geospatial information.[6,8,9] Airborne imaging can identify dairy farms and estimate CH_4 emissions directly from those facilities.[10] However, this approach requires significant resources for a regional-scale operation and has a detection limit, only capturing emissions larger than a certain level (typically 2−10 kg CH_4 h^{-1}). In addition, because the location and size of dairy facilities change over time depending on socio-economic conditions (*e.g.*, high-cost feeds), more accessible approaches to continuous monitoring of dairy emissions are necessary.

Received: December 23, 2021
Revised: March 18, 2022
Accepted: March 21, 2022
Published: April 1, 2022

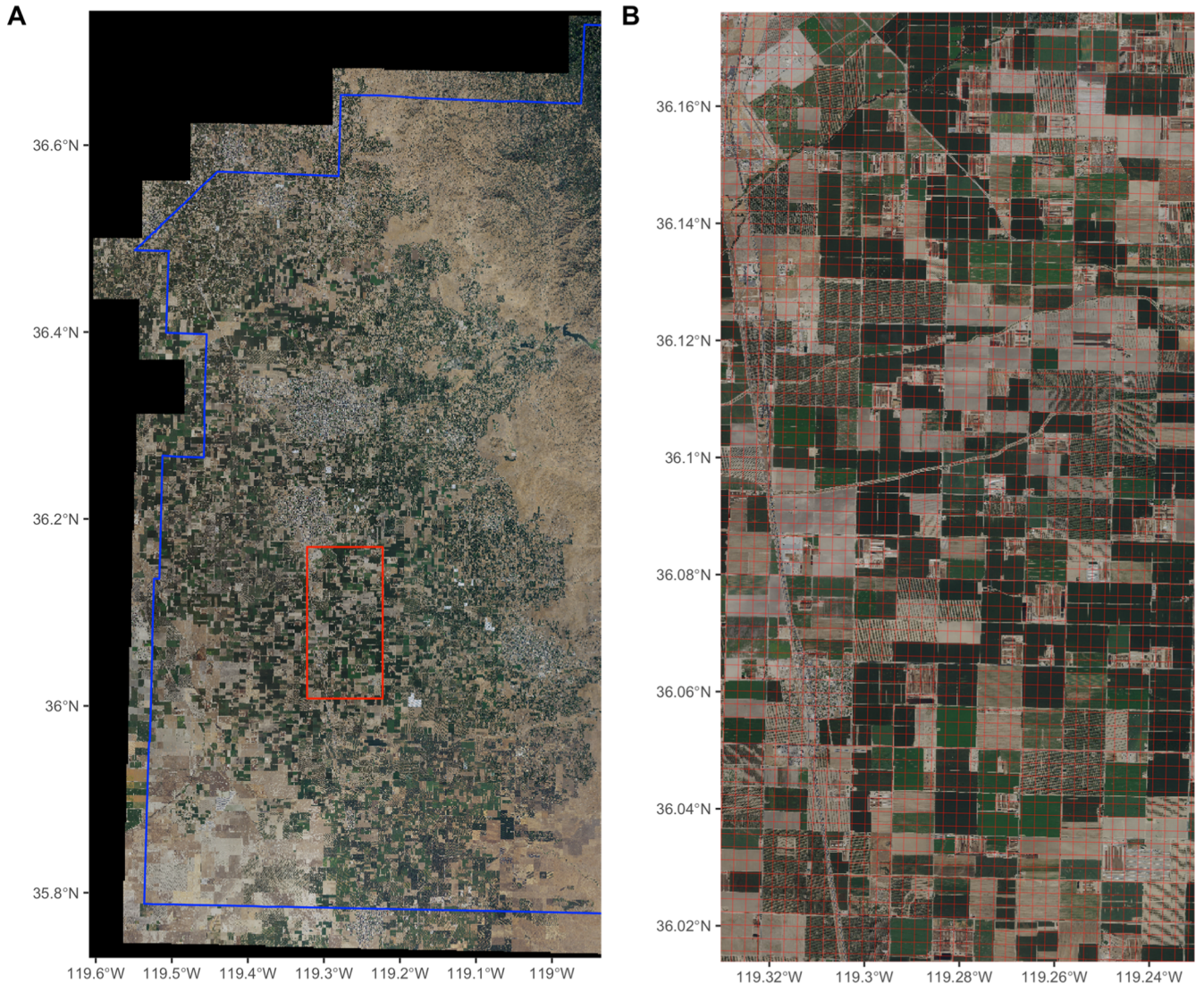

Figure 1. Example NAIP imagery: (A) downloaded NAIP imagery for California's Tulare County and (B) zoom-in view of a subset region of (A) with the grid of tile polygons overlaid. In (A), the blue line represents Tulare County's boundary. We download NAIP imagery only for the areas where active dairy operations are occurring to reduce the number of images to be processed (*e.g.*, excluding the Sierra foothill region). The red rectangle in (A) shows the bounding box for the area shown in (B). In (B), the red square polygons represent the bounding boxes of individual image tiles into which we divide the entire imagery inside the red rectangle shown in (A).

This work develops a prediction system for dairy enteric and manure CH_4 emissions by combining expert knowledge in GHG emissions with artificial intelligence (AI). Utilizing aerial imagery produced annually, we apply state-of-the-art AI methods to predict dairies' location and herd size in California's San Joaquin Valley (SJV), which accounts for the vast majority of the state's dairy emissions.[4,6] We then estimate spatially explicit dairy CH_4 emissions by combining the AI-predicted herd size with known emission factors (EFs).

This work describes a method to update dairy emissions in a timely fashion when new imagery is available. For example, applying our AI system to the aerial imagery from the National Agriculture Imagery Program (NAIP) used in this study can update dairy CH_4 emissions annually. Because we focus on estimating emissions at the annual scale comparable to existing bottom-up inventories such as California's state inventory and Vista-CA,[11] this work does not attempt to simulate the short-duration dynamic variability of dairy CH_4 emissions. Recently, Marklein *et al.*[11] updated California dairies' spatial information, manually identifying facilities. Although manual identification of dairy farms' location and size by human visual inspection is likely more accurate than the current AI algorithms, it requires considerable human effort. This work offers a low-cost method to identify dairy farms' location and size at the same time as imagery availability and to estimate the dairy population, subsequently updating spatially resolved emissions in combination with the estimated population and EFs. Thus, this work is likely to influence future emission quantification efforts directly, including atmospheric inverse modeling based on ground-based (*e.g.*, Jeong *et al.*[6]) or satellite (*e.g.*, Turner *et al.*[12]) platforms.

2. DATA AND METHODS

2.1. Aerial Imagery Processing. Aerial imagery from NAIP is used for training our AI model. Note that we use "AI" to broadly represent the process of mimicking the human mind by machines. Later, we define the terminology for AI more specifically to be consistent with the task we implement. The

https://doi.org/10.1021/acs.est.1c08802
Environ. Sci. Technol. 2022, 56, 4849−4858

NAIP aerial imagery is acquired during the agricultural growing seasons in the continental US and is available to the public at a 0.6 m resolution.[13] Because the NAIP imagery is made available within a year of acquisition, we can essentially update dairy emissions annually using the NAIP imagery.

Figure 1A shows the NAIP imagery for Tulare County, which has the largest dairy population in California. The imagery in Figure 1A shows only the subregion of Tulare County used in this study, removing the areas (*e.g.*, pastureland at the Sierra foothills) with a low probability of dairy farms' presence. Note that while Figure 1 shows processed images for Tulare County as an example, we process NAIP images for SJV's all eight counties (see Table S1). We process the imagery in Figure 1A into 49,884 individual image tiles, with each tile having an area of 305 × 305 m^2 (see Figure 1B for a grid of image tiles). The total number of individually processed image tiles for each county is presented in Table S1 in the Supporting Information. More details for image processing are provided in Text S1 of the Supporting Information.

To train the AI model, we need two types of images for each of the training, validation, and testing steps: a raw image (NAIP imagery in our case) and a mask (*i.e.*, a labeled image). To construct datasets for training, validation, and testing (see Table S2 for each step's number of images), we manually delineate boundaries of open (dry) lots or free stall barns among different components for a dairy facility creating boundary polygons. A free stall barn is a roofed housing structure, mostly without walls for ventilation. An open lot is an open space without vegetation but often includes shading structures or feed lanes. Many SJV dairy farms have both free stall barns and open lots (see Figures 2 and S1 for example images). Based on the analysis of data from the study of Salas *et al.*[9] (Figure S2), we assume that the dairy population for a given facility is proportional to the dairy's combined size for the free stall barn and/or the open lot where dairy cows are housed. Although this assumption may not hold in some cases, increasing the uncertainty, we note a strong correlation between our area-based population estimates and the results from human surveys[11] (see Figure 4). We estimate CH_4 emissions as a function of the dairy population and report uncertainty for CH_4 emissions only (not for the dairy population) at the state level, as in the study of Marklein *et al.*[11]

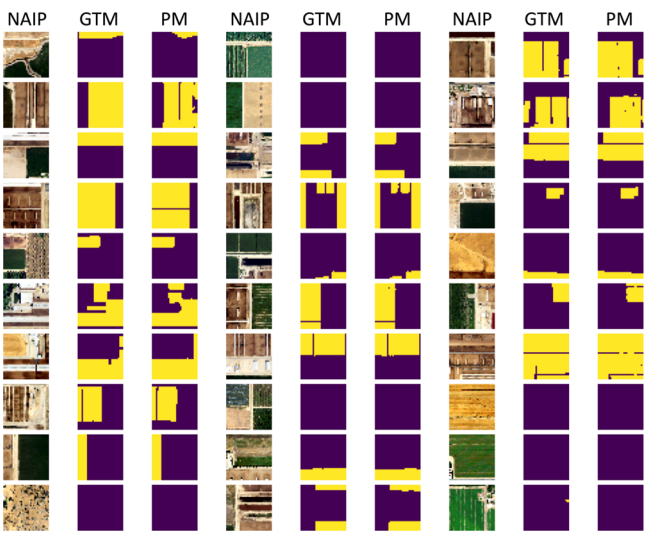

Figure 2. Example of image segmentation for dairy facilities from the testing step. Each image segmentation case consists of three components (columns in this figure). NAIP, GTM, and PM represent NAIP images, ground truth masks, and predicted masks, respectively. Thus, this figure shows a total of 30 prediction results, with each row showing three prediction cases.

2.2. Deep Learning Image Segmentation. We identify dairy facilities at the pixel level on an NAIP image using a deep learning (DL) method. DL is a subset of a family of machine learning, which is, in turn, a kind of AI. DL primarily relies on artificial neural networks (ANNs), a set of algorithms imitating the human brain's processing.[14] Here, we use AI to represent the broad approach to problem-solving using algorithms to mimic human cognitive functions while referring to DL as a class of machine learning algorithms with multiple (*i.e.*, deep) layers in the neural network. The term "deep" in DL indicates multiple layers for transforming the data from which more complex and abstract features (*e.g.*, the car's curvature rather than a simple line) are extracted progressively.

This work uses image segmentation among different DL computer vision approaches because we need to infer the probability of assigning a label to each image pixel instead of image-level classification. Using image segmentation, for example, rather than predicting whether an image includes a black bear or a grizzly bear, we are interested in predicting the pixel-level location of a black or grizzly bear in the image. Also, our 1.36 m pixel-level image segmentation is different from Handan-Nader and Ho's approach,[15] which uses an image-level classification method to detect pig and poultry feeding operations and relies on class activation mapping for facility-level detection. Our pixel-level segmentation allows for directly calculating each image's dairy farm (spatial) area, a key variable for emission estimation, by combining dairy pixels in the image. Pixel-level image segmentation applications include self-driving cars,[16] road extraction,[17] detection of deforestation,[18] and medical imaging.[19] For example, image segmentation can locate tumors, partitioning a medical image into cancer and nontumor segments.[20] We provide more details for image segmentation in Text S2.

Specific to our task of identifying dairy farms, a convolutional neural network (CNN) is used among different DL architectures. A CNN is a type of deep neural network and is used as a common choice for computer vision applications, as in this work.[21] We apply a CNN in a supervised learning setting, providing both raw images and masks to the CNN model. Thus, our CNN model learns a set of functions that map the input (image) to the output (mask) based on input−output pairs provided in the training dataset.

Among different CNNs, we apply the U-Net architecture[20] (see Text S3 for U-Net details), which is known to perform well with a relatively small number of training datasets. U-Net was initially developed for medical imaging.[20] The U-Net-based approach is useful for our study because the total number of statewide dairy farms is less than 2000,[11] from which we subsample a smaller number of images for the training process. Note that a dairy farm can be associated with multiple image tiles because of its high resolution. We combine a U-Net variant (see Figure S3 for U-Net's basic structure) with pretrained base models and image augmentation algorithms. The technique to use pretrained models is called "transfer learning". Details for transfer learning and image augmentation are described in Texts S4 and S5, respectively.

https://doi.org/10.1021/acs.est.1c08802
Environ. Sci. Technol. 2022, 56, 4849−4858

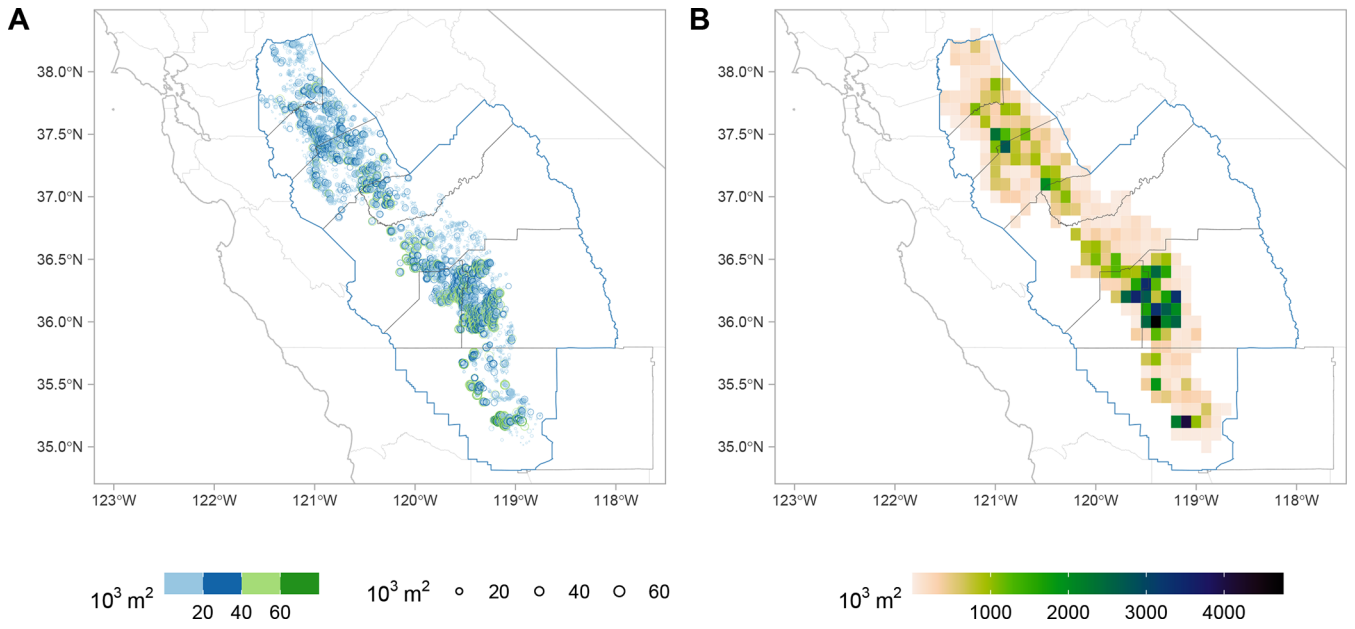

Figure 3. Estimated dairy facility area (in $\times 10^3$ m^2) by the DL model. (A) Estimated dairy facility area for individual image tiles (each tile area = 305 × 305 m^2) and (B) gridded dairy facility area at 0.1°. In (A), the circles show the locations of the 9161 (out of 316,882) image tiles identified as including dairy facilities. In (A), both the circle size and color are used to show dairy facilities' spatial area. The blue-colored polygons in (A,B) represent the San Joaquin air basin boundary, which includes eight counties (gray polygons).

For implementation, this work uses Keras (https://keras.io/), a high-level neural network interface for the well-known AI platform, TensorFlow (https://www.tensorflow.org/). For this work's specific image segmentation task, we use the Segmentation Models Python library developed for CNN image segmentation based on Keras and TensorFlow.[22] Although the specific CNN model used in this study is a U-Net variant, for the sake of simplicity, we use the term "DL model", which is a broader description for the sets of algorithms for image segmentation than the CNN model, to represent our image segmentation model.

Ten different models are evaluated based on pretrained models and non-dairy fractions. The non-dairy fraction represents the ratio of the number of non-dairy images to the total number of images in our dataset. In training the DL model, we need image tiles with non-dairy pixels only in addition to images containing dairy pixels. This is because the DL model uses both dairy and non-dairy images as inputs while processing 316,882 image tiles for the entire SJV. Overall, we find that the models using dairy and non-dairy images together perform better than those using only dairy images. We present a complete list of evaluation results for each combination of pretrained models and non-dairy fractions in Table S3 of the Supporting Information.

2.3. Dairy Facility Area Estimation. We use the dairy facility's (free stall barns and open lots) spatial area as a basis for estimating the dairy population, which is subsequently used for emission estimation combined with EFs. In practice, the facility area is used as a weight to scale the county-level dairy population. Our DL model identifies individual dairy pixels in an image tile (305 × 305 m^2 or 224 × 224 pixels) and calculates the dairy's total area within the image tile. Because we use a very high resolution of 1.36 m, we can also construct each facility's boundary. In addition, because of the high resolution, multiple image tiles can constitute a single facility. By combining facility boundaries from multiple image tiles, we construct individual facilities' boundaries and estimate the facility-level population, which is described later (see Figure S6 for the facility-level population distribution).

We aggregate the spatial areas calculated from a cluster of identified dairy pixels into a grid with a 0.1° (~10 km) resolution. A vast majority of atmospheric inverse modeling studies for CH_4 are conducted at kilometers to tens of kilometer scales.[6−8,23,24] We use this gridded area information in the subsequent analysis for dairy population and emission estimation, which are described in Texts S6 and S7 of the Supporting Information, respectively. We compare our gridded product with CALGEM[6] and Vista-CA by Marklein *et al.*[11] We note that the native resolution of the product by Marklein *et al.*[11] is at the facility level but that study uses the spatial resolution of 0.1° for comparison with other spatial inventories, including CALGEM.

3. RESULTS AND DISCUSSION

3.1. Estimation of Dairy Facility Areas. We process SJV-wide 316,882 image tiles using the DL model to separate each image tile into dairy and non-dairy pixels. We demonstrate the DL model's image segmentation capability in Figure 2. The image segmentation examples in Figure 2 are from the testing step based on the parameters optimized from the training step. Thus, the DL model has not seen the images previously, and the testing result assesses the model's performance. As shown in the figure, our DL model performs well, yielding an overall accuracy of ~0.9 (*i.e.*, ~90%; see Table S3 for accuracy). We provide more description of the image segmentation results in Text S2 in the Supporting Information.

We calculate dairy facilities' spatial areas (in m^2) from the DL model's predicted image segmentation. Recall that each image pixel has a fixed area of 1.36 × 1.36 m^2. We then predict the dairy population as a function of the dairy facility's spatial area, assuming that the dairy population is generally proportional to the facility's size based on the analysis (see Figure S2)

https://doi.org/10.1021/acs.est.1c08802
Environ. Sci. Technol. 2022, 56, 4849−4858

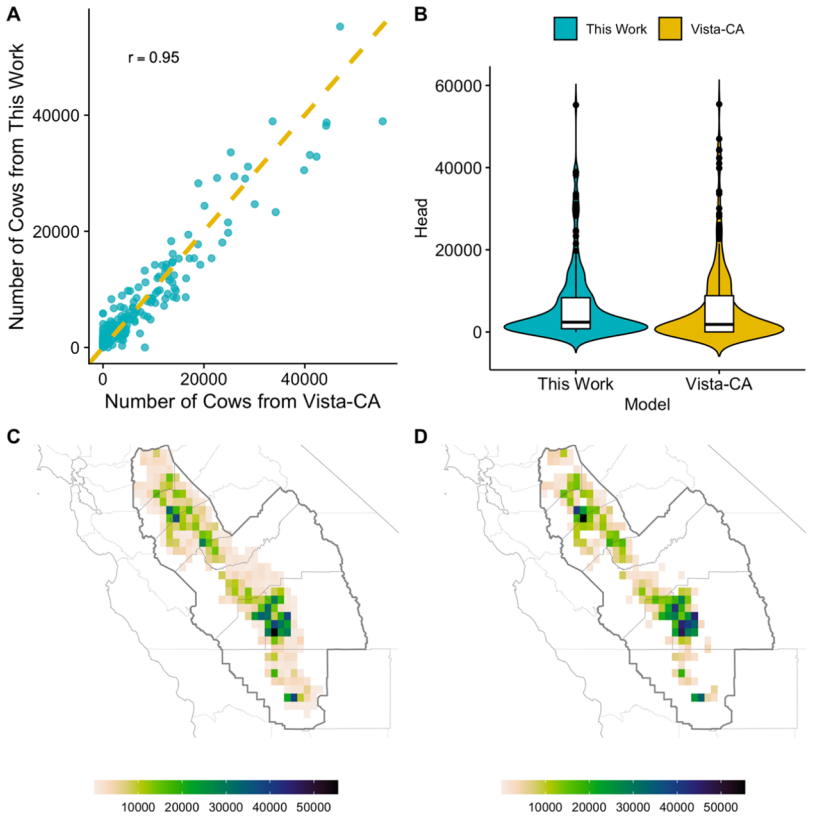

Figure 4. Comparison of dairy population estimates between the DL approach and the Vista-CA dairy product. (A) Pixel-level (at 0.1°) correlation between the DL-predicted and Vista-CA dairy populations, (B) violin plot, (C) gridded DL-predicted dairy population (at 0.1°), and (D) gridded Vista-CA dairy population (at 0.1°). In (A), the dashed line represents the 1:1 line. In (B), the violin plot shows the kernel density for the dairy population data used in (A), and boxplots are shown inside the violin plots. While the boxplot shows statistics such as median and IQR, KPD in the violin plot reveals the data's full probability distribution. Also, as shown in (B), the KPD in the violin plot is a rotated density, where the *Y*-axis represents the random variable, which is usually shown on the *X*-axis of a density plot.

using data from the study of Salas *et al.*[9] Figure 3A shows the dairy facilities' areas (*i.e.*, open lot and free stall barn areas) predicted by the DL model from the processing of 316,882 image tiles across the SJV. We estimate that 9161 image tiles are associated with dairy operations.

We show the gridded version of Figure 3A in Figure 3B, aggregating the predicted area for individual image tiles (305 × 305 m^2) into a 0.1° resolution grid. Therefore, this gridded map represents the total dairy facility area (in m^2) within each 0.1° grid pixel. We use this gridded area map to estimate the dairy population, which is subsequently used to estimate dairy CH_4 emissions. The area map indicates that large dairy clusters are located in the southern SJV that includes Tulare County, which accounts for ∼30% of SJV's total dairy population.[25] Also, Figure 3B shows a substantial concentration of dairy facilities in Stanislaus and Merced counties of the northern SJV. This area prediction result indicates that the DL model captures the SJV dairy population's overall spatial distribution expected from the US Department of Agriculture's (USDA's) county-level dairy dataset.[25] The DL-predicted county-level (aggregated) dairy farm area strongly correlates with USDA's county-level dairy population, yielding a Pearson correlation coefficient (r) of 0.97 (see Figure S4). This statistic suggests that the DL-predicted area explains ∼95% variability in the USDA dairy population. Note that the county-level dairy area is predicted by our DL model, independent from the USDA dairy population.

3.2. Spatially Explicit Dairy Population. We estimate the dairy population by apportioning USDA's county-level population[25] based on the dairy facility areas. Using USDA's county-level data essentially removes the county-level bias in the predicted population, although individual dairies' population within each county could be biased. SJV's dairy population for each county is presented in Table S7. We evaluate our DL model's capability for estimating dairy population by comparing it with the Vista-CA dairy inventory developed by Marklein *et al.*[11] Marklein *et al.* identify individual facilities through visual inspection and estimate each facility's herd size using reported data from the State Water Resources Control Board and other local sources.[11] Thus, we believe that the Vista-CA database compiled by Marklein *et al.*[11] represents the most updated and accurate spatial inventory of California's dairy population.

Figure 4A shows the 0.1° pixelwise herd population correlation between the DL model prediction and Vista-CA. In this comparison, we remove 0.1° pixels identified as non-dairy by both the DL model and Vista-CA. As shown in the figure, the prediction correlates strongly with Vista-CA, yielding a Pearson correlation coefficient (r) of 0.95. We also compare the two model results using violin plots where the kernel probability density (KPD) is shown along with boxplots (Figure 4B). While the boxplot shows summary statistics such as the median and interquartile ranges (IQRs), KPD reveals the data's full probability distribution. The two KPDs estimated using a Gaussian kernel are very similar. Also, the

https://doi.org/10.1021/acs.est.1c08802
Environ. Sci. Technol. 2022, 56, 4849−4858

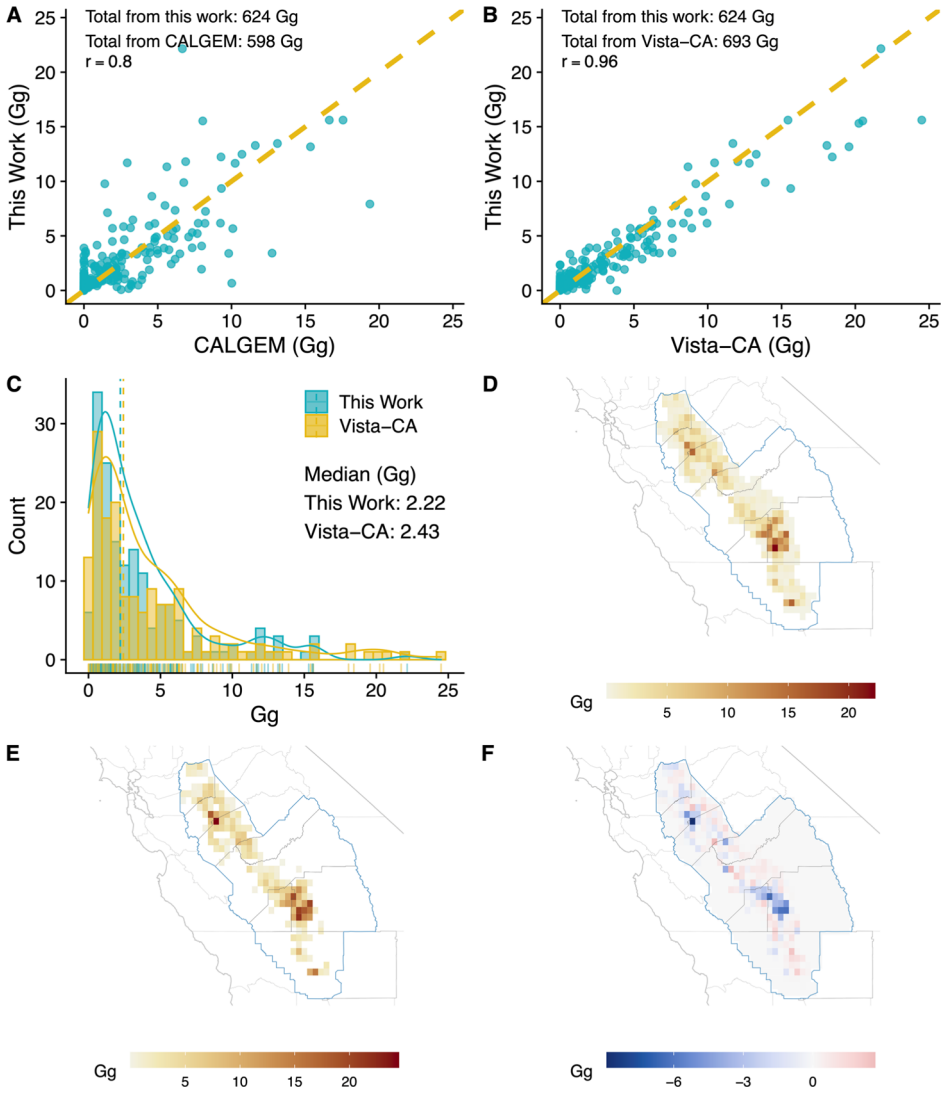

Figure 5. Comparison of annual dairy CH_4 emission estimates: (A) pixel-level (at 0.1°) correlation between the DL-predicted and CALGEM dairy CH_4 emissions (B) same as (A) but between the DL model and Vista-CA, (C) histogram comparison between the DL model and Vista-CA, (D) DL-predicted gridded CH_4 emissions (at 0.1°), (E) gridded Vista-CA emissions (at 0.1°), and (F) the difference (D minus E). In (A–C), we remove the pixels for which both the models predict zero emissions. In (A,B), the dashed line represents the 1:1 line.

two boxplots (inside the violin plots) show that the IQRs from the two models overlap, suggesting similar variance. Based on the three statistical summaries (*i.e.*, *r*, KPD, and IQR), we conclude that our DL-based population is comparable with a population estimate made by human visual inspection.

Dairy population maps (at 0.1°) from this work and Vista-CA are shown in Figure 4C,D, respectively. Consistent with the results in Figure 4A,B, the two maps show a similar spatial distribution of herd populations. Although our DL model prediction is comparable to the benchmark spatial inventory by human inspection, Vista-CA, we observe some differences between the two models. In this pixelwise comparison, the DL model predicts dairy farms in areas where Vista-CA estimates no dairy farm. In Fresno County, for example, the DL model predicts that there are dairy pixels with small populations, while Vista-CA does not show dairy farms. This is the false-positive case when the DL model misclassifies some of the non-dairy landscape for dairy farms due to similar color or texture (*e.g.*, idle fields in brown color). Furthermore, Vista-CA includes recently closed dairies, some of which may still be identified as dairy farms by the DL model. This segmentation error is a challenge to be addressed in a future work, for example, by incorporating multispectral satellite data. Ha *et al.*[26] showed that the image segmentation accuracy was improved by combining RGB images with thermal infrared information.

In addition, this work assumes that the dairy farm size is represented by the total area of the open lot and free stall barn. This approach assumes that both the open lot and the free stall barn would have the same per-unit-area population density—in reality, the two may have different densities. Our DL model does not distinguish open lots from free stall barns in the image segmentation process. Thus, this limitation in separating open lots from free stall barns may yield additional uncertainty at the facility scale, which is not accounted for in this work but can be an important research topic for future AI-based dairy inventory development.

3.3. Emission Estimation. We compare our DL-model-estimated emissions (see Text S7) with spatially explicit dairy emissions from the CALGEM emission model[6] and Vista-

https://doi.org/10.1021/acs.est.1c08802
Environ. Sci. Technol. 2022, 56, 4849–4858

CA.[11] We first compare our DL model with CALGEM, which has been used in multiple atmospheric inverse modeling studies.[6−8,24,27] Figure 5A shows that our DL-model-predicted emissions correlate well (r value = 0.80) with CALGEM in the pixelwise (0.1°) comparison. Marklein *et al.*[11] also find that Vista-CA correlates favorably with CALGEM (r value = 0.77), while they report relatively low spatial correlations with two other emission models by Hristov *et al.*[28] and Maasakkers *et al.*[29] with r values of 0.58 and 0.25, respectively. The dairy CH_4 emission estimate (624 Gg/yr) for the SJV from our DL model is slightly higher than that from CALGEM (598 Gg), which was calibrated to match the 2012 inventory from the California Air Resources Board (CARB). CALGEM's 80% level spatial correlation with our DL model suggests that the two emission models share some of the underlying spatial characteristics of SJV's dairy emissions.

We compare our DL model's emission estimates with Vista-CA (SJV total = 693 Gg) in Figure 5B. As shown in the figure, the spatial correlation at 0.1° is close to 1 with an r value of 0.96. This high correlation would mean that our DL model captures 92% ($0.96^2 = 0.92$) of Vista-CA's variability in a linear regression setting. This result demonstrates a significant potential of our DL approach, which is nearly as good at estimating spatial dairy emissions as human visual inspections. We note that the small discrepancy between our DL model and Vista-CA is a combined result of differences in the EFs applied and errors (*e.g.*, in assigning population to each pixel) from both the models.

We analyze the impact of the emission difference between DL and Vista-CA on predicted CH_4 mixing ratio concentrations, which is the critical variable in atmospheric inverse modeling. For this mixing ratio analysis, we simulate CH_4 mixing ratios using dairy emissions from the DL model and Vista-CA and compare the two results (see Figure S7). The mixing ratio comparison suggests that in a typical atmospheric inverse modeling setup, atmospheric measurements can constrain the DL-model-derived emissions as effectively as Vista-CA, given the two models' strong correlation in both spatially resolved emissions and mixing ratios. This comparison further indicates that the DL model can essentially replace Vista-CA as an alternative *a priori* emission product in a typical inverse modeling exercise for SJV's CH_4 emission quantification. We describe the mixing ratio comparison details in Text S8 of the Supporting Information (also see Figure S7).

We further evaluate our DL model's estimated emissions, comparing them with Vista-CA generated by more labor-intensive visual inspection of dairy locations and the review of dairy permit records. Figure 5C shows the histograms (*i.e.*, discrete count) and KPDs from the two models. The two models show similar probability densities, illustrating the DL model's capability to capture Vista-CA's overall emission distribution. However, as described in the population estimation, our DL model tends to overcount low-emission pixels due to classification errors while underestimating emissions for other high-flux pixels. We can better observe this result using spatial emission maps (Figure 5D−F). For example, in Fresno County, the DL model (Figure 5D) predicts relatively small emissions (<1 Gg CH_4 per pixel) near Sierra Nevada's foothill region where dairy emissions are not expected or negligible from Vista-CA, as seen in Figure 5E. This difference is because the DL model misclassifies some non-dairy pixels (with a similar color and texture to dairy facilities) as dairy pixels. The difference plot in Figure 5F shows that the DL model generally underestimates emissions from the dairy hot spots. This difference is also shown in Figure 5C, where the KPD shows that Vista-CA is more right-skewed with a mean value of 4.23 Gg than the DL model (mean = 3.67 Gg).

Many factors affect the accuracy of the DL model's performance for image segmentation. The technical factors include model architecture (*e.g.*, the structure of the CNN), the pretrained model, and the DL modeling platform (*e.g.*, TensorFlow). Image-related factors (*e.g.*, image quality and the number of training images) can be more significant players in the DL model performance than technical factors.[30] This work only implemented a limited number of combinations from the technical and image-related factors, and the model performance may be associated with this limitation. For example, the disagreement between our DL model and Vista-CA is likely attributable to the relatively small number of training datasets, even though we used image augmentation. Future studies are necessary to improve the prediction accuracy by exploring a more comprehensive set of technical factors as well as more training and testing datasets.

Although our primary goal is to evaluate the DL model's performance against Vista-CA, we conduct a simple comparison between DL model emission estimates and those using the Next Generation Airborne Visible/Infrared Imaging Spectrometer (AVIRIS-NG).[10] For comparison with our work, we derive CH_4 emissions for 130 dairy facilities from 204 dairy/manure distinct sources quantified by AVIRIS-NG using a hierarchical spatial clustering method implemented in R (https://cran.r-project.org, specifically R's stats package). While we report annual emissions, AVIRIS-NG emissions are estimated from short-duration field campaigns. The emission comparison between DL and AVIRIS-NG is presented in Figure S5 of the Supporting Information with some caveats, including the temporal scale difference. AVIRIS-NG shows more superemitters relative to the DL model, while the DL model's mean (0.96 Gg; median = 0.88) is higher than that (0.83 Gg; median = 0.55) of AVIRIS-NG by 16%. In addition to the temporal scale difference, the incongruity between the two estimates may be attributed to the uncertainty in the EFs and the DL model's dairy population estimates as well as AVIRIS-NG's estimation uncertainty. We also note that AVIRIS-NG's estimates are associated with detection limits (typically >2 kg/h).

We estimate the SJV-wide uncertainty in dairy CH_4 emissions using the uncertainty estimate from the US EPA (Environmental Protection Agency) inventory.[31] We use simplified EFs (in units of CH_4 kg/head) for both enteric fermentation and manure management. Thus, our method for uncertainty estimation is similar to the first approach used by Marklein *et al.*,[11] which is based on the US EPA inventory. The EPA inventory estimates the emission uncertainty range (as a percentage deviation from the central estimate) to be from −11 to 18% and −18 to 20% for enteric fermentation and manure management, respectively. As in the studies of Marklein *et al.*[11] and Jeong *et al.*,[32] we assume that this fractional uncertainty from EPA applies to our regional scale analysis. Because our image segmentation is associated with ∼10% error (see Table S3), we add this additional 10% error to the EPA's fractional uncertainty for enteric fermentation and manure management. We sample the dairy cow population with 10% uncertainty due to segmentation errors and then multiply the sampled population by EFs, which are sampled

https://doi.org/10.1021/acs.est.1c08802
Environ. Sci. Technol. 2022, 56, 4849−4858

from lognormal distributions (see Text S9 in the Supporting Information). Based on EPA's uncertainty and the additional 10% segmentation error, we estimate that SJV dairy CH_4 emissions are 496−763 Gg/yr at 95% confidence (see Figure S8). In this estimation, we assume lognormal distributions for both enteric and manure emissions due to the asymmetric percentage deviation from the mean. The estimation detail is presented in Text S9 of the Supporting Information.

3.4. Application for Anaerobic Digestion Deployment. Anaerobic digestion (AD) is the degradation and stabilization of organic substrates in the absence of oxygen by microorganisms. These processes produce CH_4-rich biogas that can be used as an energy source directly or cleaned to generate biomethane for vehicle use or pipeline injection. Interest in AD of manure for biogas production and waste management has increased with policies, such as Senate Bill 1383, mandating the reduction of short-lived climate pollutants.[3] Dairy digesters, which include closed systems as well as covered lagoons, are mature technologies. However, these technologies have high upfront capital costs and must meet complex regulations and standards. Deployment in locations where clusters of dairies could invest in and share the infrastructure could overcome this challenge but requires dairy facilities' spatial location and size information.

The AI approach presented in this study can play an important role in overcoming this challenge, particularly offering updated spatial information of dairy facilities and their size. Dairy clusters have been identified through public reporting and used in financial feasibility analysis to determine project viability.[33] Our AI approach could be applied to detect clusters of dairy facilities where waste or biogas can be processed together to achieve economies of scale. Used in combination with geospatial analysis techniques, such an approach would facilitate the down-selection of dairy clusters based on essential characteristics such as proximity to roads and natural gas transmission pipelines. The rapid development of deployment and monitoring guidance-based AI approaches can dramatically improve the return on investment (ROI) and the life-cycle CH_4 reduction performance of the state's investments in AD.

Reviewing the large (90th percentile) farms, we find 162 farms with herd sizes ranging from 2334 to 8433 cows (see Figure S6 for the farm-level herd size distribution). Assuming a 0.3 m^3 CH_4 per kg volatile solid loaded biomethane production factor and AD's 75% efficiency for CH_4 capture,[11] we estimate 247 Gg CH_4/yr biomethane production for the SJV. Biomethane production factors used in the literature range from 0.24 to 0.4 m^3 CH_4 per kg volatile solid loaded,[34,35] which results in a biomethane production for the SJV between 198 and 329 Gg CH_4/yr. We also estimate a CH_4 reduction potential of 83 Gg CH_4/yr, assuming CARB's EF for AD[4] for these large facilities. When we vary the EF for AD from 3 to 20%, reflecting low to high leakage rates,[36] the CH_4 reduction potential varies from 67 to 91 Gg CH_4/yr. Our estimate is higher than the reduction potential (26 Gg CH_4/yr) estimated by Marklein *et al.*,[11] who evaluate emissions reductions for only 100 farms that have or are scheduled to have digesters.

3.5. Potentials and Future Applications of AI. For the first time, we introduce an AI-based low-cost approach to estimating dairy CH_4 emissions that can be directly used in atmospheric inverse modeling studies for emission quantification. We estimate SJV's dairy CH_4 emissions for 2018 using aerial imagery and DL AI. Our work demonstrates an AI-based approach's capability to develop spatially resolved emissions more frequently and efficiently. We estimate SJV's dairy CH_4 emissions, which correlate very well (>95%) with those of Vista-CA compiled by human visual surveys. As a direct application of our approach, we estimate the biomethane production and AD's CH_4 emission reduction from the 90th percentile facilities predicted by our DL model.

We see the potential that our DL approach can be improved beyond the demonstrated results in this work. The result can be refined by combining the images used in this work (*i.e.*, natural color images) with multispectral satellite images[26] and different pretrained models. Particularly, multispectral images can provide more information (*e.g.*, thermal property and moisture content) in addition to those (*e.g.*, texture and color) extracted from visible spectral images. We have tested only a limited number of model architectures from the AI technology perspective, although we trained our DL model using 10 different combinations of pretrained models and non-dairy fractions. The image segmentation result (Table S3) suggests that training the DL model including images without dairy farms improves the segmentation accuracy compared to the case with dairy images only (*i.e.*, a non-dairy fraction of 0). Model training with more non-dairy images with similar color and texture to dairy images could reduce the misclassification error (*e.g.*, confusion between dairy and idle lands), which may constitute the object of future studies. Furthermore, the U-Net architecture employed in this work yields comparable results to Vista-CA using only ∼2000 images (Table S2) for model training. Our result reinforces the previous finding that U-Net performs well with a relatively small number of training datasets,[20] which can be a significant implication for future earth science applications of DL where preparing training datasets is costly.

Our result suggests that the methods developed in this work can be applied to other future works. For instance, performing image segmentation on lagoons as an additional separate category would better characterize the manure management system. This additional feature would require preparing the training dataset where anaerobic lagoons are masked differently from open lots or free stall barns. Also, our methods can be used to estimate emissions for other GHG sectors. For example, we could apply DL models to detect the natural gas infrastructure, power plants, large manufacturing facilities, and landfills using very high-resolution satellite imagery. Currently, many inventories rely on emitters' voluntary reporting, and compiling spatiotemporal data from the emitters is done manually.[37,38] Expanding on this work, we can use various AI technologies to detect unreported emission sources, add spatiotemporal information to the reported raw data, and automate many of the reporting processes.[15]

While we only show a fraction of what AI technology can do to solve pressing climate change problems, our work suggests that AI can perform what humans used to do to address environmental challenges, with a comparable quality but in an automated manner. Furthermore, we note that our approach could offer the greatest benefit at the continental or global scale where human inspection is costly and challenging to apply repeatedly.

■ ASSOCIATED CONTENT

Supporting Information

The Supporting Information is available free of charge at https://pubs.acs.org/doi/10.1021/acs.est.1c08802.

https://doi.org/10.1021/acs.est.1c08802
Environ. Sci. Technol. 2022, 56, 4849−4858

Image processing, image segmentation, U-Net structure, transfer learning, image augmentation, dairy population, emission estimation, CH_4 mixing ratio simulation, uncertainty estimation, the example of image−mask pairs, comparison of DL emission estimates with AVIRIS-NG, facility-level comparison, the number of images used, model training scores, USDA dairy statistics, and CARB EFs (PDF)

AUTHOR INFORMATION

Corresponding Author

Seongeun Jeong − *Lawrence Berkeley National Laboratory, Berkeley, California 94720, United States;* orcid.org/0000-0003-2032-0127; Email: sjeong@lbl.gov

Authors

Marc L. Fischer − *Lawrence Berkeley National Laboratory, Berkeley, California 94720, United States;* orcid.org/0000-0001-7956-2361

Hanna Breunig − *Lawrence Berkeley National Laboratory, Berkeley, California 94720, United States;* orcid.org/0000-0002-4727-424X

Alison R. Marklein − *University of California, Riverside, California 92521, United States*

Francesca M. Hopkins − *University of California, Riverside, California 92521, United States*

Sebastien C. Biraud − *Lawrence Berkeley National Laboratory, Berkeley, California 94720, United States*

Complete contact information is available at: https://pubs.acs.org/10.1021/acs.est.1c08802

Funding

This work was partially supported by the University of California, Office of the President, Laboratory Fee Research Program (grant LFR-18-548581), Contractor Supporting Research (CSR) funding at LBNL, and a grant from the California Energy Commission (SUMMATION project, agreement number PIR-17-015), all operated at LBNL under contract no. DE-AC02-05CH11231.

Notes

The authors declare no competing financial interest.

ACKNOWLEDGMENTS

We thank Samir Touzani for offering valuable suggestions in processing aerial images and many helpful discussions for deep learning. We also thank LBNL's Lawrencium PI Compute Allowance (PCA) program for running the WRF-STILT models on the Lawrencium cluster. The authors' views and opinions expressed herein do not necessarily state or reflect those of the United States Government or any agency thereof or The Regents of the University of California. The results in this paper do not necessarily represent the views of the California Energy Commission (CEC) or the State of California. CEC, the State of California, its employees, contractors, and subcontractors make no warranty, express or implied, and assume no legal liability for the information in this paper; nor does any party represent that the uses of this information will not infringe upon privately owned rights. This paper has not been approved or disapproved by CEC, nor has CEC passed upon the accuracy or adequacy of the information in this paper. The NAIP data are available at https://www.fsa.usda.gov/programs-and-services/aerial-photography/imagery-programs/naip-imagery/. The image and mask datasets used for model training, validation, and testing are available at https://sites.google.com/lbl.gov/calgem. The Vista-CA dairy spatial inventory is available from the Oak Ridge National Laboratory Distributed Active Archive Center for Biogeochemical Dynamics (https://doi.org/10.3334/ORNLDAAC/1814). The code for Keras' image segmentation model is available at https://github.com/qubvel/segmentation_models.

REFERENCES

(1) Intergovernmental Panel on Climate Change. *Climate Change 2013—The Physical Science Basis: Working Group I Contribution to the Fifth Assessment Report of the Intergovernmental Panel on Climate Chang.*; Cambridge University Press: Cambridge, 2014.

(2) Legislative Information Senate Bill No. 32. https://leginfo.legislature.ca.gov/faces/billNavClient.xhtml?bill_id=201520160SB32 (accessed April 30, 2021).

(3) Legislative Information Senate Bill No. 1383. https://leginfo.legislature.ca.gov/faces/billTextClient.xhtml?bill_id=201520160SB1383 (accessed 30 April 2021).

(4) CARB Documentation of California's 2000-2018 GHG Inventory. https://ww2.arb.ca.gov/applications/california-ghg-inventory-documentation (accessed April 30, 2021).

(5) USDA Milk Production. https://www.nass.usda.gov/Publications/Todays_Reports/reports/mkpr0220.pdf (accessed 30 April 2021).

(6) Jeong, S.; Newman, S.; Zhang, J.; Andrews, A. E.; Bianco, L.; Bagley, J.; Cui, X.; Graven, H.; Kim, J.; Salameh, P.; LaFranchi, B. W.; Priest, C.; Campos-Pineda, M.; Novakovskaia, E.; Sloop, C. D.; Michelsen, H. A.; Bambha, R. P.; Weiss, R. F.; Keeling, R.; Fischer, M. L. Estimating methane emissions in California's urban and rural regions using multitower observations. *J. Geophys. Res. Atmos.* **2016**, *121*, 13031−13049.

(7) Cui, Y. Y.; Vijayan, A.; Falk, M.; Hsu, Y.-K.; Yin, D.; Chen, X. M.; Zhao, Z.; Avise, J.; Chen, Y.; Verhulst, K.; Duren, R.; Yadav, V.; Miller, C.; Weiss, R.; Keeling, R.; Kim, J.; Iraci, L. T.; Tanaka, T.; Johnson, M. S.; Kort, E. A.; Bianco, L.; Fischer, M. L.; Stroud, K.; Herner, J.; Croes, B. A Multiplatform Inversion Estimation of Statewide and Regional Methane Emissions in California during 2014-2016. *Environ. Sci. Technol.* **2019**, *53*, 9636−9645.

(8) Jeong, S.; Hsu, Y.-K.; Andrews, A. E.; Bianco, L.; Vaca, P.; Wilczak, J. M.; Fischer, M. L. A multitower measurement network estimate of California's methane emissions. *J. Geophys. Res. Atmos.* **2013**, *118*, 11339−11351.

(9) Salas, W.; Li, C.; Mitloehner, F.; Pisano, J. *Developing and Applying Process-Based Models for Estimating Greenhouse Gas and Air Emissions from California Dairies*; California Energy Commission, 2009.

(10) Duren, R. M.; Thorpe, A. K.; Foster, K. T.; Rafiq, T.; Hopkins, F. M.; Yadav, V.; Bue, B. D.; Thompson, D. R.; Conley, S.; Colombi, N. K.; Frankenberg, C.; McCubbin, I. B.; Eastwood, M. L.; Falk, M.; Herner, J. D.; Croes, B. E.; Green, R. O.; Miller, C. E. California's methane super-emitters. *Nature* **2019**, *575*, 180−184.

(11) Marklein, A. R.; Meyer, D.; Fischer, M. L.; Jeong, S.; Rafiq, T.; Carr, M.; Hopkins, F. M. Facility-scale inventory of dairy methane emissions in California: implications for mitigation. *Earth Syst. Sci. Data* **2021**, *13*, 1151−1166.

(12) Turner, A. J.; Jacob, D. J.; Wecht, K. J.; Maasakkers, J. D.; Lundgren, E.; Andrews, A. E.; Biraud, S. C.; Boesch, H.; Bowman, K. W.; Deutscher, N. M.; Dubey, M. K.; Griffith, D. W. T.; Hase, F.; Kuze, A.; Notholt, J.; Ohyama, H.; Parker, R.; Payne, V. H.; Sussmann, R.; Sweeney, C.; Velazco, V. A.; Warneke, T.; Wennberg, P. O.; Wunch, D. Estimating global and North American methane emissions with high spatial resolution using GOSAT satellite data. *Atmos. Chem. Phys.* **2015**, *15*, 7049−7069.

(13) NAIP The National Agriculture Imagery Program. https://www.fsa.usda.gov/programs-and-services/aerial-photography/imagery-programs/naip-imagery/ (accessed May 10, 2020).

(14) Goodfellow, I.; Bengio, Y.; Courville, A. *Deep Learning*; MIT Press, 2016.
(15) Handan-Nader, C.; Ho, D. E. Deep learning to map concentrated animal feeding operations. *Nat. Sustain.* **2019**, *2*, 298−306.
(16) Hussain, R.; Zeadally, S. Autonomous Cars: Research Results, Issues, and Future Challenges. *Commun. Surv. Tutorials, IEEE* **2019**, *21*, 1275−1313.
(17) Zhang, Z.; Liu, Q.; Wang, Y. Road Extraction by Deep Residual U-Net. *Geosci. Rem. Sens. Lett. IEEE* **2018**, *15*, 749−753.
(18) de Bem, P.; de Carvalho Junior, O.; Fontes Guimarães, R.; Trancoso Gomes, R. Change Detection of Deforestation in the Brazilian Amazon Using Landsat Data and Convolutional Neural Networks. *Rem. Sens.* **2020**, *12*, 901.
(19) Comelli, A.; Coronnello, C.; Dahiya, N.; Benfante, V.; Palmucci, S.; Basile, A.; Vancheri, C.; Russo, G.; Yezzi, A.; Stefano, A. Lung Segmentation on High-Resolution Computerized Tomography Images Using Deep Learning: A Preliminary Step for Radiomics Studies. *J. Imaging* **2020**, *6*, 125.
(20) Ronneberger, O.; Fischer, P.; Brox, T. U-Net: Convolutional Networks for Biomedical Image Segmentation. Springer International Publishing: Cham, 2015; pp 234−241.
(21) Albawi, S.; Mohammed, T. A.; Al-Zawi, S. Understanding of a convolutional neural network. *2017 International Conference on Engineering and Technology (ICET)*; 2017; Vol. *21*−*23*, pp 1−6. DOI: 10.1109/icengtechnol.2017.8308186
(22) Yakubovskiy, P. Segmentation Models https://github.com/qubvel/segmentation_models [Online], 2019 (accessed March 5, 2020).
(23) Jeong, S.; Zhao, C.; Andrews, A. E.; Bianco, L.; Wilczak, J. M.; Fischer, M. L. Seasonal variation of CH_4 emissions from central California. *J. Geophys. Res. Atmos.* **2012**, *117*, D11306.
(24) Jeong, S.; Cui, X.; Blake, D. R.; Miller, B.; Montzka, S. A.; Andrews, A.; Guha, A.; Martien, P.; Bambha, R. P.; LaFranchi, B.; Michelsen, H. A.; Clements, C. B.; Glaize, P.; Fischer, M. L. Estimating methane emissions from biological and fossil-fuel sources in the San Francisco Bay Area. *Geophys. Res. Lett.* **2017**, *44*, 486−495.
(25) USDA California cattle county estimates. https://www.nass.usda.gov/Statistics_by_State/California/Publications/County_Estimates/2016/201705LvstkCActy.pdf (accessed December 12, 2020).
(26) Ha, Q.; Watanabe, K.; Karasawa, T.; Ushiku, Y.; Harada, T. MFNet: Towards Real-Time Semantic Segmentation for Autonomous Vehicles with Multi-Spectral Scenes. *2017 IEEE/RSJ International Conference on Intelligent Robots and Systems (IROS)*; 2017; pp 5108−5115.
(27) Johnson, M. S.; Xi, X.; Jeong, S.; Yates, E. L.; Iraci, L. T.; Tanaka, T.; Loewenstein, M.; Tadić, J. M.; Fischer, M. L. Investigating seasonal methane emissions in Northern California using airborne measurements and inverse modeling. *J. Geophys. Res. Atmos.* **2016**, *121*, 13753−13767.
(28) Hristov, A. N.; Harper, M.; Meinen, R.; Day, R.; Lopes, J.; Ott, T.; Venkatesh, A.; Randles, C. A. Discrepancies and Uncertainties in Bottom-up Gridded Inventories of Livestock Methane Emissions for the Contiguous United States. *Environ. Sci. Technol.* **2017**, *51*, 13668−13677.
(29) Maasakkers, J. D.; Jacob, D. J.; Sulprizio, M. P.; Turner, A. J.; Weitz, M.; Wirth, T.; Hight, C.; DeFigueiredo, M.; Desai, M.; Schmeltz, R.; Hockstad, L.; Bloom, A. A.; Bowman, K. W.; Jeong, S.; Fischer, M. L. Gridded National Inventory of U.S. Methane Emissions. *Environ. Sci. Technol.* **2016**, *50*, 13123−13133.
(30) Yip, M. Y. T.; Lim, G.; Lim, Z. W.; Nguyen, Q. D.; Chong, C. C. Y.; Yu, M.; Bellemo, V.; Xie, Y.; Lee, X. Q.; Hamzah, H.; Ho, J.; Tan, T.-E.; Sabanayagam, C.; Grzybowski, A.; Tan, G. S. W.; Hsu, W.; Lee, M. L.; Wong, T. Y.; Ting, D. S. W. Technical and imaging factors influencing performance of deep learning systems for diabetic retinopathy. *NPJ Digit. Med* **2020**, *3*, 40.
(31) US EPA Inventory of U.S. Greenhouse Gas Emissions and Sinks: 1990-2018. https://www.epa.gov/ghgemissions/inventory-us-greenhouse-gas-emissions-and-sinks-1990-2018 (accessed 20 December 2020).
(32) Jeong, S.; Millstein, D.; Fischer, M. L. Spatially explicit methane emissions from petroleum production and the natural gas system in California. *Environ. Sci. Technol.* **2014**, *48*, 5982−5990.
(33) USDA Economic Feasibility of Dairy Digester Clusters in California: A Case Study. https://archive.epa.gov/region9/organics/web/pdf/cba-session2-econ-feas-dairy-digester-clusters.pdf (accessed February 10, 2021).
(34) Mangino, J.; Bartram, D.; Brazy, A. Development of a methane conversion factor to estimate emissions from animal waste lagoons. *US EPA's 17th Annual Emission Inventory Conference*; Atlanta, Georgia, 2001.
(35) Daniel-Gromke, J.; Rensberg, N.; Denysenko, V.; Stinner, W.; Schmalfuß, T.; Scheftelowitz, M.; Nelles, M.; Liebetrau, J. Current Developments in Production and Utilization of Biogas and Biomethane in Germany. *Chem. Ing. Tech.* **2018**, *90*, 17−35.
(36) Flesch, T. K.; Desjardins, R. L.; Worth, D. Fugitive methane emissions from an agricultural biodigester. *Biomass Bioenergy* **2011**, *35*, 3927−3935.
(37) Carranza, V.; Rafiq, T.; Frausto-Vicencio, I.; Hopkins, F. M.; Verhulst, K. R.; Rao, P.; Duren, R. M.; Miller, C. E. Vista-LA: Mapping methane-emitting infrastructure in the Los Angeles megacity. *Earth Syst. Sci. Data* **2018**, *10*, 653−676.
(38) Rafiq, T.; Duren, R. M.; Thorpe, A. K.; Foster, K.; Patarsuk, R.; Miller, C. E.; Hopkins, F. M. Attribution of methane point source emissions using airborne imaging spectroscopy and the Vista-California methane infrastructure dataset. *Environ. Res. Lett.c* **2020**, *15*, 124001.

https://doi.org/10.1021/acs.est.1c08802
Environ. Sci. Technol. 2022, 56, 4849−4858